GA–A27913

APPLYING THE RADIATING DIVERTOR APPROACH TO INNOVATIVE TOKAMAK DIVERTOR CONCEPTS

by

T.W. PETRIE, C.J. LASNIER, A.W. LEONARD, J.G. WATKINS, S.L. ALLEN, J.M. CANIK, M.E. FENSTERMACHER, J.R. FERRON, R.J, GROEBNER, C.T. HOLCOMB, A.W. HYATT, E. KOLEMEN, R.J. LA HAYE, T.C. LUCE, R. MAINGI, A.G. McLEAN, R.A. MOYER, W.M. SOLOMON, V.A. SOUKHANOVSKII, and F. TURCO

SEPTEMBER 2014

GENERAL ATOMICS

DISCLAIMER

GA–A27913

APPLYING THE RADIATING DIVERTOR APPROACH TO INNOVATIVE TOKAMAK DIVERTOR CONCEPTS

by
T.W. PETRIE, C.J. LASNIER,* A.W. LEONARD, J.G. WATKINS,† S.L. ALLEN,* J.M. CANIK,‡ M.E. FENSTERMACHER,* J.R. FERRON, R.J, GROEBNER, C.T. HOLCOMB,* A.W. HYATT, E. KOLEMEN,¶ R.J. LA HAYE, T.C. LUCE, R. MAINGI,¶ A.G. McLEAN,* R.A. MOYER,§ W.M. SOLOMON,¶ V.A. SOUKHANOVSKII,* and F. TURCO#

This is a preprint of a paper to be presented at the Twenty-Fifth IAEA Fusion Energy Conf., October 13-18, 2014 in Saint Petersburg, Russia.

*Lawrence Livermore National Laboratory, Livermore, California.
†Sandia National Laboratories, Livermore, California.
‡Oak Ridge National Laboratory, Oak Ridge, Tennessee.
¶Princeton Plasma Physics Laboratory, Princeton, New Jersey.
§University of California San Diego, La Jolla, California.
#Columbia University, New York, New York.

Work supported by
the U.S. Department of Energy
under DE-FC02-04ER54698, DE-AC52-07NA27344,
DE-AC04-94AL85000, DE-AC05-00OR22725, DE-AC02-09CH11466,
DE-FG02-07ER54917 and DE-FG02-04ER54761

GENERAL ATOMICS PROJECT 30200
SEPTEMBER 2014

GENERAL ATOMICS

Applying the Radiating Divertor Approach to Innovative Tokamak Divertor Concepts

EX/P2-26

T.W. Petrie[1], C.J. Lasnier[2], A.W. Leonard[1], J.G. Watkins[3], S.L. Allen[2], J.M. Canik[4], M.E. Fenstermacher[2], J.R. Ferron[1], R.J. Groebner[1], C.T. Holcomb[2], A.W. Hyatt[1], E. Kolemen[5], R.J. La Haye[1], T.C. Luce[1], R. Maingi[5], A.G. McLean[2], R.A. Moyer[6], W.M. Solomon[5], V.A. Soukhanovskii[2], and F. Turco[7]

[1]*General Atomics, P.O. Box 85608, San Diego, CA 92186-5608, USA*
[2]*Lawrence Livermore National Laboratory, Livermore, CA 94550, USA*
[3]*Sandia National Laboratories, P.O. Box 5800, Albuquerque, NM 87185, USA*
[4]*Oak Ridge National Laboratory, P.O. Box 2008, Oak Ridge, TN 37831, USA*
[5]*Princeton Plasma Physics Laboratory, PO Box 451, Princeton, NJ 08543-0451, USA*
[6]*University of California San Diego, La Jolla, CA 92093-0417, USA*
[7]*Columbia University, 2960 Broadway, New York, NY 10027, USA*
e-mail contact of main author: petrie@fusion.gat.com

Abstract. Recent DIII-D experiments evaluated the effectiveness of three innovative tokamak divertor concepts in reducing divertor heat flux under radiating divertor conditions. These concepts are: (1) high performance standard double-null divertor (DND) plasmas, (2) high performance double-null "snowflake" (SF-DN) plasmas, and (3) single-null H-mode plasmas with different isolation from their divertor targets. Significant reductions in both divertor heat flux and electron temperature were observed in both standard DND and SF-DN high performance discharges under comparable neon/deuterium-based radiating divertor conditions, while at the same time maintaining favorable high performance metrics, e.g., $\beta_N \cong 3.0$ and $H_{98(Y,2)} \cong 1.4$. The high performance metrics for SF-DN plasmas were comparable to those of more conventional DND plasmas, although impurity accumulation in the former was typically higher, e.g., ≥20%. The peak heat flux ($q_{\perp,P}$) was significantly reduced by extending the parallel connection length ($L_{\|\text{-XPT}}$) in the scrape-off layer between the X-point and divertor targets, both under radiating- and non-radiating divertor conditions. Extending ($L_{\|\text{-XPT}}$) was also shown to facilitate access to lower core density as well as lower neon accumulation in the core. In general, all three concepts are attractive, achieving reduced divertor heat flux while preserving good H-mode confinement.

1. Introduction

Future highly-powered tokamaks will require a means to reduce potentially damaging power loading at the divertor targets. Several previous investigations have shown that significant reductions in heat loading are possible by enhancing the radiated power upstream of the divertor targets through a combination of deuterium and impurity injection, e.g., "puff-and-pump" [1–4]. Other possible solutions would rely more on ways that exploit divertor geometry to achieve heat flux reduction, such as extending the parallel connection length of the divertor legs [5] or reconfiguring the divertor to a non-conventional divertor shape, e.g., "Snowflake" [6]. In this paper, we report on the possible additional benefits to divertor heat flux reduction when the puff-and-pump radiating divertor approach is combined with "advanced" divertor configurations. The advanced divertor geometries that we consider are: (1) high triangularity double-null divertor (DND) plasmas [Fig. 1(a)], (2) high performance double-null "Snowflake" (SF-DN) plasmas [Fig. 1(b)], and (3) single-null plasmas having different parallel connection lengths in the scrape-off layer (SOL) from their X-point to outer divertor target $L_{\|\text{-XPT}}$ [Fig. 1(c,d)].

The DND shape is commonly considered as the model for "advanced" high performance tokamak plasmas because of its advantages in confinement and stability over conventional single-null shapes offered by its higher triangularity [7,8]. Previously on DIII-D, the "puff-and-pump" radiating divertor approach, which used either argon or neon as seed impurities,

was applied to DND H-mode plasmas, producing significant reductions in divertor heating with only modest degradation in energy confinement, e.g., Ref. [4]. For the DND plasmas discussed in this paper in Sec. 3.1, we examine the response of high performance DND plasmas, i.e., those with normalized plasma beta $\beta_N \approx 3$ and normalized energy confinement time $H_{98(y,2)} \approx 1.35$, across combinations of deuterium and neon impurity fueling in order to identify the most promising way forward.

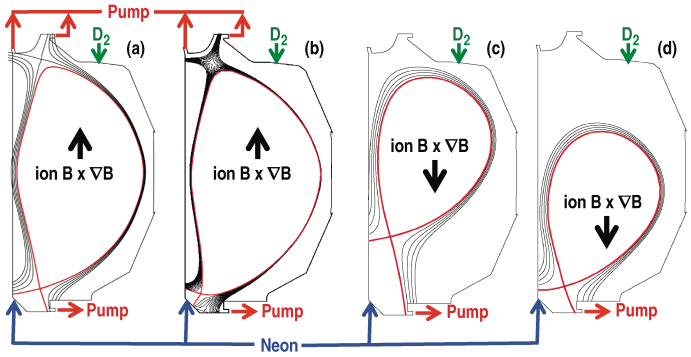

Fig. 1. The plasma cross-sections and the poloidal locations for the deuterium and neon injectors and particle pumping: (a) *DND*, (b) SF-DN, (c) longer outer divertor leg ($L_{\parallel\text{-XPT}}$ = 26 m) and (d) the corresponding shorter outer divertor leg ($L_{\parallel\text{-XPT}}$ = 18 m).

The Snowflake divertor has been shown to be effective in dissipating heat flux at the divertor target for single-null discharges in both NSTX [9] and DIII-D [10]. The Snowflake divertor used here is configured by adding a second X-point near the outer divertor target (i.e., "Snowflake-minus" [6]). This raises the poloidal flux expansion along the outer divertor target ($F_{EXP\text{-}OD}$). In turn, the incoming power flow is more evenly dispersed across the outer divertor compared with a conventional divertor configuration, which does not have this second divertor X-point. In this paper, we directly compare heat flux reduction and overall plasma performance of the Snowflake with that of the DND (Sec. 3.2), under both low density and high-density (radiating divertor) conditions. As with the DND, these SF-DN configurations have high triangularity.

Previous studies [11] on DIII-D have shown that extending $L_{\parallel\text{-XPT}}$ produces broader heat flux profiles with lower peak heat fluxes at the outer divertor target, in spite of the $F_{EXP\text{-}OD}$ of the shorter $L_{\parallel\text{-XPT}}$ being considerably greater, e.g., 3.2 versus 5.6. SOLPS modeling of those data indicate that cross-field transport is an important consideration for these plasmas and that perpendicular transport gains in importance relative to parallel transport as $L_{\parallel\text{-XPT}}$ is extended. In Sec. 3.3, we investigate the degree to which increasing $L_{\parallel\text{-XPT}}$ under radiating divertor conditions can facilitate further reductions in heat flux at the divertor target.

2. Experimental Arrangement

The experimental setup for the DND configuration [Fig. 1(a)] is characterized by: (a) slight magnetic bias toward the lower divertor, i.e., dRsep = -5 mm, (b) the ion $\boldsymbol{B}$ x $\boldsymbol{\nabla B}$ drift direction toward the upper divertor, (c) active particle exhaust by two cryopumps located in the upper and the one cryopump in lower divertor, (d) neon and deuterium gases are injected, respectively, into the private flux region of the lower divertor and upstream into the main chamber, and (e) β_N (or plasma stored energy) is held steady by a combination of neutral beam under feedback control and applied electron cyclotron heating (ECH) that is constant.

The SF-DN configuration used in this study [Fig. 1(b)] also has a slight magnetic bias toward the lower divertor similar to that of the DND. The upper (secondary) divertor and the lower inner divertor shapes were very similar to the DND shape. The extra null in the SF-DN lower outer divertor provided the only significant difference with the DND geometry. Otherwise the experimental setup and approach were identical to the DND case above.

Figures 1(c) and 1(d) show two identically shaped main plasmas that have significantly different isolations from their respective lower divertor targets. The vertical distance from their X-points to their outer divertor target were 75 cm and 25 cm, respectively. These

distances correspond to parallel connection lengths measured from the X-point down to the outer divertor target ($L_{||\text{-XPT}}$) of 26 m and 18 m, respectively. The horizontal poloidal distances from their X-points to their vertical inner divertor targets were approximately 15 cm, which would correspond to parallel connection lengths of 6–8 m. When discussing $L_{||\text{-XPT}}$, we are referencing to the flux surface that lies 1.5 mm radially outboard of the outer midplane separatrix flux surface.

Because the DIII-D vessel is protected by graphite tiles, carbon is the main intrinsic impurity. Heat flux information in the lower divertor is based on infrared camera measurements. The peak heat flux in the upper outer divertor was determined from measurements by a second infrared camera. Electron density and temperature at the divertor targets were based on Langmuir probe measurements and upstream density and temperature by Thomson scattering. These measurements were taken between type-1 edge localized modes (ELMs). Neon density profiles inside the main plasma were based on charge-exchange recombination analysis. The current profiles and the resulting value of safety factor on-axis were determined by motional Stark effect polarimetry.

3. Results

3.1. High performance DND plasmas

Density Scan: Pronounced changes in divertor and core plasma conditions were observed as core density was increased. Details for these shots are given in column 1 (lowest density "control" shot) through column 3 (highest density) of Table 1. As density increased, β_N was largely maintained by raising neutral beam power, but the normalized energy confinement time ($H_{98(Y,2)}$) decreased by ≈20%. Between ELMs, peak heat flux at the inner target ($q_{\perp,LOW,IN,BE}$) and at the outer target ($q_{\perp,LOW,OUT,BE}$) in the lower divertor decreased by ≈80% and ≈40%, respectively, from low to high density. However, the peak heat flux at the upper outer divertor target ($q_{\perp,OUT,UP,BE}$) *increased*. Raising core density produced a large increase in ELM frequency (ν_{ELM}) and perhaps not coincidently a sizable reduction in the peak heat flux at all three divertor targets *during* an ELMing event. The peak density at each of the three divertor targets (between ELMs) increased strongly with increasing core density (and Γ_{D2}). The corresponding peak electron temperatures at the lower inner ($T_{IN,LOW,BE}$) and lower outer ($T_{OUT,LOW,BE}$) divertor targets dropped sharply with increasing core density, while the peak electron temperature at the upper outer target ($T_{OUT,UP,BE}$) remained fairly steady.

Total radiated power ($P_{RAD,TOT}$) increased strongly as core density and Γ_{D2} were increased. Almost 60% of P_{INPUT} was radiated at the highest density (column 3), although only ≈20% of P_{INPUT} was radiated inside the main plasma. Bolometric-inversions indicate that half of the increase in $P_{RAD,TOT}$ occurred in the lower (primary) divertor, while ≈30% and ≈20% of this increase came from the main plasma and upper (secondary) divertor, respectively. Power flow across the separatrix into the SOL in the high density, radiating divertor case (column 3) was larger than in that the low density case (column 1), but this "additional" power to the lower divertor was more than offset by a strong increase in localized radiated power in the lower divertor. The increase in power to the upper outer divertor during the radiating divertor phase was roughly comparable to the increase in localized radiated power in the upper divertor, so that differences in $q_{\perp,UP,OUT}$ (and $T_{P,UP,OUT}$) should not be as pronounced. These results appear to be the consequences of imposing the constraint that β_N stay constant and of the *increase* in the radiated power primarily being from the lower divertor.

Table 1. Operating conditions for the radiating divertor study using DND

	Control	Moderate Γ_{D2} and n_e	High Γ_{D2} and n_e	$\Gamma_{D2} + \Gamma_{NE}$	Γ_{NEON} Only
Γ_{D2} (Torr l/s)	10	56	103	56	0
Γ_{NEON} (Torr l/s)	0.55	0.55	0.55	5.3	5.3
Density (10^{19} m^{-3})	3.75	4.50	5.20	5.03	4.36
β_N	2.91	2.89	2.73	2.90	2.92
P_{INPUT} (MW)	9.8	10.6	12.3	9.8	10.3
$H_{98(Y,2)}$	1.33	1.24	1.08	1.28	1.31
q_0	1.60	1.41	1.08	1.08	1.17
ν_{ELM} (Hz)	80	126	165	92	55
$q_{\perp,IN,LOW,BE}$ (MW/m^2)	1.5	1.4	0.33	0.2	1.0
$q_{\perp,OUT,LOW,BE}$ (MW/m^2)	3.5	3.3	2.2	1.6	2.6
$q_{\perp,OUT,UP,BE}$ (MW/m^2)	1.0	1.4	1.9	1.2	1.0
$q_{\perp,IN,LOW,ELM}$ (MW/m^2)	3.8	3.3	1.33	2.5	4.7
$q_{\perp,OUT,LOW,ELM}$ (MW/m^2)	5.6	5.2	3.2	3.2	5.8
$q_{\perp,OUT,UP,ELM}$ (MW/m^2)	3.6	2.6	2.6	2.5	4.7
$n_{IN,LOW,BE}$ (10^{19} m^{-3})	2.1	4.8	11.0	6.7	2.0
$n_{OUT,LOW,BE}$ (10^{19} m^{-3})	2.5	4.0	5.7	4.2	2.3
$n_{OUT,UP,BE}$ (10^{19} m^{-3})	1.6	3.8	6.9	3.0	1.6
$T_{IN,LOW,BE}$ (eV)	31	20	16	18	22
$T_{OUT,LOW,BE}$ (eV)	40	33	26	20	28
$T_{OUT,UP,BE}$ (eV)	14	14	16	14	14
$P_{RAD,TOT}$ (MW)	3.05	3.70	6.91	5.78	4.41
$P_{RAD,CORE}$ (MW)	0.98	1.10	2.15	1.86	1.51
Z_{eff} (ρ=0.7)	1.81	1.58	1.55	3.36	4.84
n_D/n_e (ρ=0.7)	0.860	0.898	0.897	0.706	0.535

Neon injection only: We now examine changes in divertor and core plasma conditions by primarily raising the neon injection rate Γ_{NEON} from a trace level (column 1) to a perturbing level (column 5). Even though $P_{RAD,TOT}$ and the core radiated power $P_{RAD,CORE}$ were significantly higher in the perturbative Γ_{NEON} case, $H_{98(Y,2)}$ was maintained. Both $q_{\perp,IN,LOW,BE}$ and $q_{\perp,OUT,LOW,BE}$ in the column 5 case were reduced 25-35% and $q_{\perp,OUT,UP,BE}$ was unchanged in the upper divertor. However, the downside of this approach is clear. Lower power flow through the pedestal translated to a lower ν_{ELM} in the neon-only injection case (column 5), which, in turn, led to more intense ELMing events when they occurred with higher peak heat fluxes at all three divertor targets. When compared with the control case in column 1, the Z_{eff} in column 5 was considerably higher (4.8 vs 1.8) and the fraction of the deuterium fuel ion in the core n_D/n_e (0.86 vs 0.54) considerably lower.

Neon and deuterium: A combination of a "moderate" deuterium gas puff rate Γ_{D2} (as in column 2) and a perturbative neon injection rate Γ_{NEON} (as in column 5) yielded the most optimal results overall in terms of maintaining elevated β_N and $H_{98(Y,2)}$ while reducing heat flux both during *and* between ELMs (column 4). The combination of increasing Γ_{D2} (which would increase ν_{ELM}) and perturbative Γ_{NEON} (which would decrease ν_{ELM}) produced an ELM frequency only modestly different from that of the control case (column 1). Although Z_{eff} here was considerably lower than in the pure neon injection case, Z_{eff} was still elevated with respect to cases 1–3.

The buildup of an injected impurity inside the main plasma for different combinations of Γ_{D2} and Γ_{NEON} had similarities (and differences) to that found in previous studies. For trace neon injection, raising Γ_{D2} was found to be beneficial in lowering n_{NEON} (ρ=0.7) in the main plasma by about ≈35% over the range in Γ_{D2} [Fig. 2(a)]. Two processes that are likely contributing to this result: (1) reduced leakage of neon into the core by an increasingly strong flow of deuterium ions into the divertor ("puff-and-pump") and (2) the greater

difficulty of the injected neon in passing through the pedestal into the plasma core, as increasing Γ_{D2} produced a factor of two increase in ν_{ELM}. However, previous radiating divertor studies [12] with similarly shaped ELMing H-mode plasmas over a similar range in Γ_{D2} showed a factor of *four* reduction of the injected impurity density. The principal differences were: (1) Particle pumping was done on both the outer and inner divertor targets and (2) the injected impurity (argon) had a factor of two smaller ionization mean-free path based on divertor density and temperature (and hence less chance to escape the divertor). Experiments to resolve the relative contributions of impurity selection to the need for a second divertor pump are presently planned. We also found that n_{NEON} (ρ=0.7) increased roughly linearly with increasing Γ_{NEON}, but at a lower rate for higher values of Γ_{D2} [Fig. 2(b)]. For both Fig. 2(a,b), the principal intrinsic impurity carbon n_{CAR} (ρ=0.7) was largely insensitive to Γ_{D2} and Γ_{NEON}.

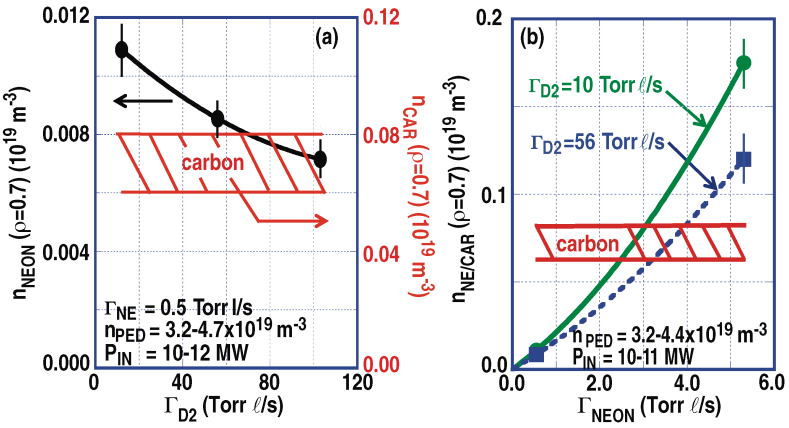

Fig. 2. (a) Neon density n_{NEON} and carbon density n_{CAR} at ρ=0.7, as a function of Γ_{D2}; Γ_{NEON} is at a trace level. (b) n_{NEON} and n_{CAR} at ρ=0.7 as a function of Γ_{NEON} for two values of Γ_{D2}. Parameters: I_P = 1.0 MA, P_{INJ} = 10–12 MW, β_N = 2.7–2.9, $H_{98(Y,2)}$ = 1.10–1.35.

High performance DND plasmas in DIII-D frequently run with a minimum value of their safety factor on axis q_0 well above unity in order to exploit the expected improvements in energy confinement and β limits [13]. However, maintaining a *steady* elevated q_0 under strongly radiating divertor plasma conditions was not achieved (Table 1). Whether this was the result of the inherent cooling in the plasma pedestal region (and consequential current profile peaking) or simply non-optimized operation is still to be determined.

3.2. High performance Snowflake plasmas

High performance SF-DN plasmas largely mirrored the high performance characteristics of DNDs under both radiating- and non-radiating divertor conditions, as shown in Fig. 3. For the first 3.5 s, plasmas were identically prepared in the DND shape; for t > 3.5 s, the plasma either remained in the DND shape (black) or was drawn into the SF-DN shape (red). For either case, both β_N and $H_{95(Y,2)}$ were maintained at high performance levels, 3.0 and 1.35, respectively. This was not unexpected, because these SF-DN and DND plasmas have very similar poloidal cross-sections, upper and lower triangularities, and q_{95}. Both DND and SF-DN maintained q_0 above unity.

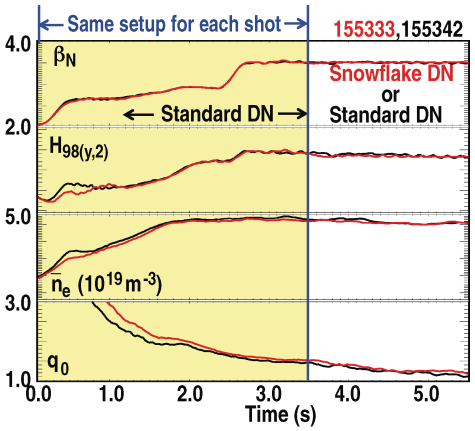

Fig. 3. Comparison of SF-DN (red) with DND (black) under non-radiative divertor conditions. (a) β_N, (b) $H_{98(Y,2)}$, (c) line-averaged density, and (d) q_0. Parameters: I_P = 1.0 MA, $q_{95} \cong 5$, and $P_{IN} \cong 10$ MW.

Since their lower *inner* divertor geometry was nearly identical, both SF-DN and DND heat flux profiles at their respective *inner* divertor targets were similar, both prior to and during the radiating phases, as discussed in Ref. [14]. On the other hand, Ref. [14] showed that an important advantage of the SF-DN lies in a much larger poloidal flux expansion at its

lower *outer* divertor target, i.e., $F_{EXP-OD} \cong 28$ for the SF-DN versus ≅9 for the DND, producing prior to puff-and-pump a factor of 2.3 times lower peak heat flux at the outer divertor target with the SF-DN than with the DND. In addition, $q_{\perp,p}$ at the lower outer divertor target for the SF-DN in the *non-radiating divertor* case was still lower than $q_{\perp,p}$ for the corresponding DND in the *radiating divertor case*, highlighting a distinct advantage of SF-DN in heat flux reduction.

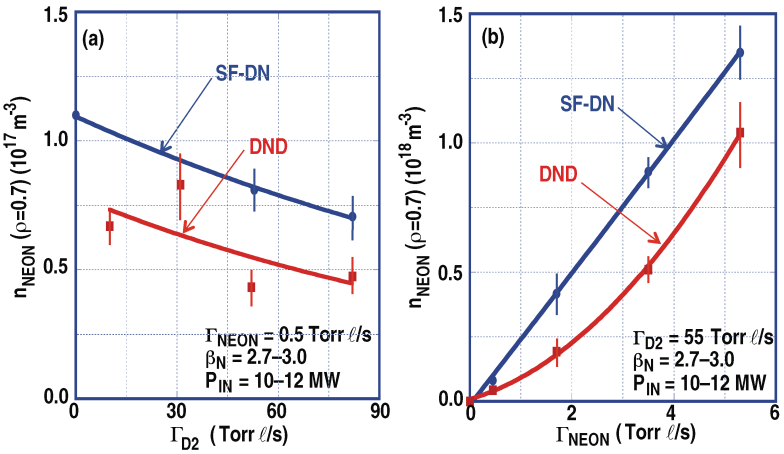

Fig. 4. $n_{NEON}(\rho=0.7)$ is shown as a function of (a) Γ_{D2} and (b) Γ_{NEON}.

However, there was a potential downside to the SF-DN. Neon accumulation in the SF-DN was 30%–40% higher than comparable DND cases, as shown in the Γ_{D2} and Γ_{NEON} scans in Fig. 4(a) and 4(b), respectively. This result, at least in part, was a consequence of particle pumping of the lower outer divertor target typically being at least a factor of two lower for SF-DNs than for comparable DNDs due to the former's large F_{EXP-OD}, although particle exhaust by the *upper* divertor pumps was still appreciable for both configurations. Consistent with this, the line-averaged density was also uniformly higher in the SF-DN cases. Hence, an improved way to efficiently pump a SF-DN configuration must be an important next step in assessing its application to future tokamak devices.

3.3. Effect of parallel connection length

There was a significantly greater reduction in $q_{\perp,p}$ for the short $L_{||\text{-XPT}}$ (= 18 m) case than for the long $L_{||\text{-XPT}}$ (=26 m) case over the wide range in operating conditions studied [Fig. 5(a,b)]. Except at the lowest Γ_{D2} and core density in Figs 5(a) and 5(b), their outer strike points were partially detached. For the attached cases ("No RD" in Table 2), which had nearly the same $\bar{n}_e$, the peak heat flux for the shorter $L_{||\text{-XPT}}$ case was ≅80% higher than for the longer $L_{||\text{-XPT}}$ case. By geometric argu-ments alone $q_{\perp,p}$ would be expected to have *lower* divertor heat flux for this short $L_{||\text{-XPT}}$ case, since the poloidal flux expansion F_{EXP-OD} at its outer divertor target was larger than the long $L_{||\text{-XPT}}$, i.e., 4.2 vs 2.7. (Power balance measurements suggest that there was a <10% difference

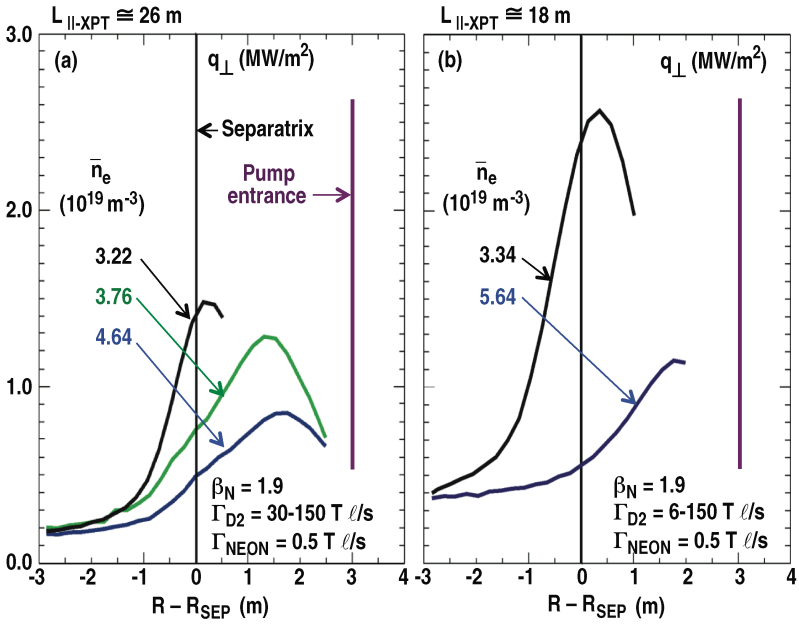

Fig. 5. Heat flux profiles with respect to the outer divertor separatrix at selected densities for both (a) $L_{||\text{-XPT}}$ = 18 m and (b) $L_{||\text{-XPT}}$ = 26 m cases. Parameters: I_P = 1.0 MA, β_N =1.9, and P_{INPUT} = 7–9 MW, and trace neon.

in the power flow going to their respective outer divertor targets.) This result is consistent with a previous study [11] that showed that the broadening effect of combining cross-field transport along SOL field lines with a greater parallel connection length in the longer $L_{\parallel\text{-XPT}}$ case could have a stronger influence on heat flux profile broadening than the larger $F_{EXP\text{-}OD}$ in a shorter $L_{\parallel\text{-XPT}}$ case. It is also clear from Fig. 5(a) and Fig. 5(b) that this advantage was extended into detached regimes, such that comparable heat flux reduction was achievable at much lower core density in the longer $L_{\parallel\text{-XPT}}$ case. Table 2 compares a long $L_{\parallel\text{-XPT}}$ case with its short $L_{\parallel\text{-XPT}}$ case counterpart under both non-radiating (NO-RD) and strong radiating divertor (RD) conditions by using both deuterium and perturbing neon gas injection. The longer $L_{\parallel\text{-XPT}}$ case had lower $q_{\perp,P}$ outer target in NO-RD and RD cases.

Table 2. Long versus short parallel connection length cases with and without strong radiating conditions

	High X-point		Low X-point	
	No RD	RD	No RD	RD
$L_{\parallel\text{-XPT}}$	26	26	18	18
β_N	1.9	1.9	1.9	1.0
$F_{EXP\text{-}OD}$	2.7	2.7	4.2	4.2
Γ_{D2} (Torr l/s)	30	150	6.0	150
Γ_{NEON} (Torr l/s)	0.4	5.3	0.4	5.3
P_{INPUT} (MW)	6.4	9.2	6.6	8.9
$q_{\perp,P}$ (MW/m^2)	1.5	0.4	2.6	0.8
H_{89P}	1.55	1.30	1.55	1.30
n_e/n_G	0.35	0.54	0.36	0.56
Z_{eff}	1.44	1.84	1.30	1.86

H-mode plasmas that have longer $L_{\parallel\text{-XPT}}$ also had lower core density at comparable Γ_{D2}, as shown in Fig. 6. The possible reason(s) for this is under investigation, but one factor may be that greater isolation of the core plasma from a source of strong recycling (and core fueling) along the outer divertor target. Moreover, the longer $L_{\parallel\text{-XPT}}$ case, which has lower $F_{EXP\text{-}OD}$, provided at least 20% higher particle exhaust due to better "focusing" of particles in front of the lower divertor cryopump.

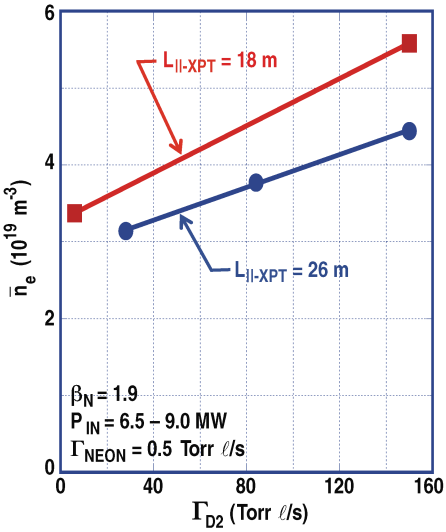

Fig. 6. Line-averaged density vs Γ_{D2} for $L_{\parallel\text{-XPT}}$ = 18 m and 26 m cases. Γ_{NEON} is at a trace level.

Trace neon accumulation in the main plasma shows an *absolute* reduction in neon density of 6–8 times over the range in Γ_{D2} for both $L_{\parallel\text{-XPT}}$ cases [Fig. 7(a)]. As with the DND, this drop in neon with increasing Γ_{D2} could be the result of reduced leakage of neon into the core by an increasingly strong flow of deuterium ions into the divertor, as well as the factor of 2-3 increase in ν_{ELM} over the range in Γ_{D2} for both $L_{\parallel\text{-XPT}}$ cases. In addition, n_{NEON} (ρ=0.7) was approximately a factor of two lower in the longer $L_{\parallel\text{-XPT}}$ than in the shorter $L_{\parallel\text{-XPT}}$ case, given similar Γ_{D2}. As with the lower plasma density found in the longer $L_{\parallel\text{-XPT}}$ case [Fig. 6(a)], the lower neon density for the long $L_{\parallel\text{-XPT}}$ cases in Fig. 7(a) may be related to the greater isolation of the core plasma from one of the sources of neon recycling and to more effective neon removal by the lower divertor cryopump from in the above paragraph for differences in deuterium fueling of the main plasma.

However, this advantage of the long $L_{\parallel\text{-XPT}}$ cases in maintaining lower impurity accumulation was lost, as higher values of Γ_{NEON} were used [Fig. 7(b)]. The cause of this is not at present clear. One possibility under investigation is that the perturbing levels of neon injection in both $L_{\parallel\text{-XPT}}$ cases is sufficient to cool the inner divertor target to partial detachment, and "cold" recycling plasma is so close to the core plasma, the neon particles have a much easier route into the core. That the ion $\mathbf{B}\times\nabla\mathbf{B}$ in these cases was toward the lower divertor would facilitate this cooling of the inner divertor region [15].

4. Preliminary Conclusions

This study represents an initial step in systematically examining potential solutions to the high power loading expected in future generation high-powered tokamaks. We find that all three concepts examined here are attractive, with good heat flux control and energy confinement, particu-larly when combined with radiating divertor techniques. Downsides to these approaches were also identified. For example, impurity contamination of the core plasma (and resulting "fuel dilution") can be an important drawback under certain DND and SF-DN radiating divertor scenarios, although we found that a judicious addition of deuterium puffing to impurity (neon) injection ameliorated impurity contamination while largely maintaining good heat flux reduction and energy confinement. We have identified that core contamination could present a more difficult challenge to the SF-DN configuration, because the higher poloidal flux expansion at its outer divertor target would make particle pumping (and impurity removal) more problematic. Optimal particle exhaust of the SF-DN is an issue that will be addressed in future DIII-D experiments.

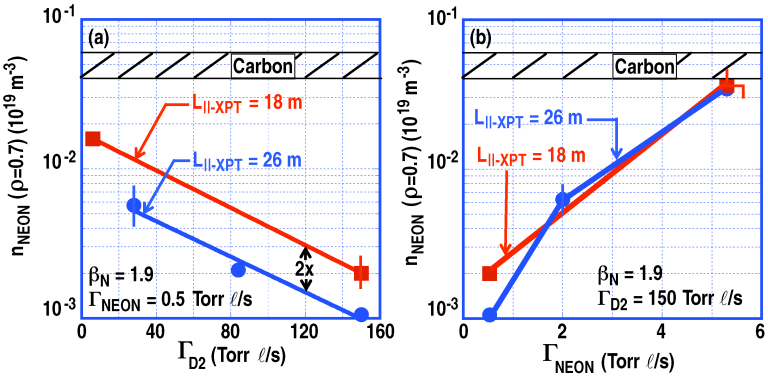

Fig. 7. (a) Neon density at ρ=0.7 as a function of Γ_{D2} for $L_{||\text{-XPT}}$ = 18 m and 26 m cases. Γ_{NEON} is at a trace level. (b) n_{NEON} (ρ=0.7) as a function of Γ_{NEON} for $L_{||\text{-XPT}}$ = 18 m and 26 m cases.

Increasing $L_{||\text{-XPT}}$ reduced $q_{\perp,P}$ at the outer divertor target under non-radiating divertor conditions and an additional factor of 2–3 times reduction when radiating divertor conditions were applied. We also found that plasmas with shorter $L_{||\text{-XPT}}$ had higher core density under similar Γ_{D2}. This was likely the result of a combination of having outboard recycling (and fueling source) closer to the main plasma and of having higher poloidal flux expansion at the outer target for the short $L_{||\text{-XPT}}$ case, which in turn would reduce the particle pumping effectiveness (analogous to SF-DN cases). However, this latter problem might be resolvable by better control over poloidal flux expansion near the pumping ports.

This material is based upon work supported by the U.S. Department of Energy, Office of Science, Office of Fusion Energy Sciences, using the DIII-D National Fusion Facility, a DOE Office of Science user facility, under Award DE-FC02-04ER54698, DE-AC05-00OR22725, DE-AC04-94AL85000, DE-AC52-07NA27344, and DE-FG02-07ER54917.

References

[1] WADE, M.R., *et al.*, Nucl. Fusion. **38** (1998) 1839.
[2] RAPP J., *et al.*, Nucl. Fusion **44** (2004) 312.
[3] KALLENBACH A., *et al.*, J. Nucl. Mater. **337–339** (2005) 732.
[4] PETRIE T.W., *et al.*, J. Nucl. Mater. **363–365** (2007) 416.
[5] KOTSCHENREUTHER M., Phys. Plasmas **14** (2007) 072502.
[6] RYUTOV D., Phys. Plasmas **14** (2007) 06452.
[7] OSBORNE T.H., *et al.*, Plasma Phys. Control. Fusion **42** (2000) A175.
[8] FERRON J.R., et al., Phys. Plasmas **12** (2005) 056126.
[9] SOUKHANOVSKII V.A., *et al.*, Phys. Plasmas **19** (2012) 082504.
[10] HILL D.N., *et al.*, Nucl. Fusion **53** (2013) 104001.
[11] PETRIE T.W., *et al.*, Nucl. Fusion **53** (2013) 113024.
[12] PETRIE T.W., *et al.*, "Compatibility of the radiating divertor with high performance plasmas in DIII-D," Proc. of the 21st IAEA Fusion Energy Conf., Chengdu, China, 2006.
[13] TURNBULL A.D., *et al.*, Phys. Rev. Lett. **74** (1995) 718.
[14] PETRIE T.W., *et al.*, "Application of the radiating divertor approach to innovative tokamak concepts," Proc. 21st Int. Conf. on Plasma Surface Interactions, Kanazawa, Japan, 2014, to be published in J. Nucl. Mater.
[15] PETRIE T.W., *et al.*, Nucl. Fusion **48** (2008) 045010.